JACS
JOURNAL OF THE AMERICAN CHEMICAL SOCIETY
pubs.acs.org/JACS
Article

Metal–Organic Framework Based Hydrogen-Bonding Nanotrap for Efficient Acetylene Storage and Separation

Yingxiang Ye,● Shikai Xian,● Hui Cui, Kui Tan, Lingshan Gong, Bin Liang, Tony Pham, Haardik Pandey, Rajamani Krishna, Pui Ching Lan, Katherine A. Forrest, Brian Space, Timo Thonhauser, Jing Li,* and Shengqian Ma*

Cite This: *J. Am. Chem. Soc.* 2022, 144, 1681–1689

Read Online

ACCESS | Metrics & More | Article Recommendations | Supporting Information

ABSTRACT: The removal of carbon dioxide (CO_2) from acetylene (C_2H_2) is a critical industrial process for manufacturing high-purity C_2H_2. However, it remains challenging to address the tradeoff between adsorption capacity and selectivity, on account of their similar physical properties and molecular sizes. To overcome this difficulty, here we report a novel strategy involving the regulation of a hydrogen-bonding nanotrap on the pore surface to promote the separation of C_2H_2/CO_2 mixtures in three isostructural metal–organic frameworks (MOFs, named MIL-160, CAU-10H, and CAU-23, respectively). Among them, MIL-160, which has abundant hydrogen-bonding acceptors as nanotraps, can selectively capture acetylene molecules and demonstrates an ultrahigh C_2H_2 storage capacity (191 $cm^3\ g^{-1}$, or 213 $cm^3\ cm^{-3}$) but much less CO_2 uptake (90 $cm^3\ g^{-1}$) under ambient conditions. The C_2H_2 adsorption amount of MIL-160 is remarkably higher than those for the other two isostructural MOFs (86 and 119 $cm^3\ g^{-1}$ for CAU-10H and CAU-23, respectively) under the same conditions. More importantly, both simulation and experimental breakthrough results show that MIL-160 sets a new benchmark for equimolar C_2H_2/CO_2 separation in terms of the separation potential (Δq_{break} = 5.02 mol/kg) and C_2H_2 productivity (6.8 mol/kg). In addition, *in situ* FT-IR experiments and computational modeling further reveal that the unique host–guest multiple hydrogen-bonding interaction between the nanotrap and C_2H_2 is the key factor for achieving the extraordinary acetylene storage capacity and superior C_2H_2/CO_2 selectivity. This work provides a novel and powerful approach to address the tradeoff of this extremely challenging gas separation.

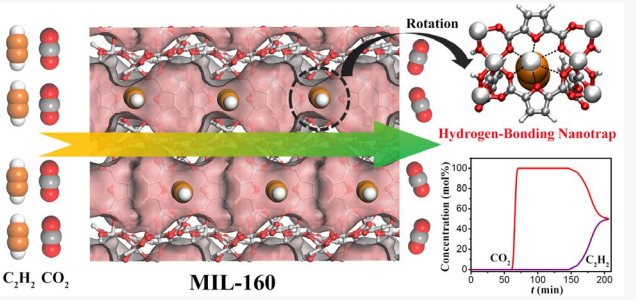

INTRODUCTION

Gas separation and purification are crucial processes in the chemical industry to manufacture polymers, fuel, and plastics.[1−4] Acetylene (C_2H_2) is not only an important gaseous fuel but also a fundamental building block for modern commodity chemicals.[5] However, impurity components (e.g., CO_2) are inevitably produced during the production of acetylene.[6] Since these two gas molecules have very similar molecular sizes/shapes (C_2H_2, 3.34 × 3.32 × 5.70 Å^3; CO_2, 3.33 × 3.18 × 5.36 Å^3) and physical properties (boiling points: C_2H_2, 189.3 K; CO_2, 194.7 K),[7] the separation of a C_2H_2/CO_2 mixture is one of the most challenging separation tasks.[8−10] In recent years, a gas separation approach based on the physical adsorption of porous adsorbents has attracted extensive attention due to its low cost and energy-saving prospects,[11−15] in comparison to the traditionally energy intensive cryogenic distillation technology.[16]

The emerging metal–organic frameworks (MOFs)[17−23] feature high modularity, large surface areas, and abundant functionality, in comparison with traditional solid adsorbents (e.g., zeolite and activated carbon).[24,25] They can be readily constructed by combining metal ions/clusters with organic linkers through coordination linkages[26,27] and have been well demonstrated to be promising in addressing many important gas separations (e.g., flue gas, olefin/paraffin).[28−35] It is a daunting challenge for a porous adsorbent in gas separation and purification to have both a high storage capacity and a high selectivity, the so-called tradeoff. For instance, MOFs with a high density of open metal sites (OMS; e.g., MOF-74 and HKUST-1) can improve the storage capacity of C_2H_2; however, it has also been shown that a high affinity for CO_2 can result in lower separation selectivity.[36−39] On the other hand, several ultramicroporous MOFs exhibit a high separation selectivity of C_2H_2/CO_2 yet have a limited acetylene uptake capacity.[40−43] Therefore, there is an added value to develop an effective approach to address this tradeoff and achieve efficient separation of C_2H_2/CO_2 mixtures.

Received: October 7, 2021
Published: December 29, 2021

https://doi.org/10.1021/jacs.1c10620
J. Am. Chem. Soc. 2022, 144, 1681–1689

Due to their nearly identical kinetic diameters (ca. 3.3 Å), effective separation of a C_2H_2/CO_2 mixture cannot be achieved simply through fine-tuning the pore size, unlike the case for other gaseous mixtures (e.g., CO_2/CH_4, alkyne/alkene),[44,45] Notably, there is a significant difference in the quadrupole moments and electrostatic potentials of carbon dioxide and acetylene (-13.4×10^{-40} and $+20.5 \times 10^{-40}$ C m^2 for CO_2 and C_2H_2; Figure S1).[46,47] Thus, it is essential to fabricate specific functional sites within the porous MOFs that can preferentially bind with C_2H_2 over CO_2. Inspired by the concept of specific recognition of crown ether complexes and macrocyclic molecules (Scheme 1a),[48−50] we hypothesize that

Scheme 1. (a) Crown Ether Complex According to Pedersen[48] and (b) Selective Capture by a Hydrogen-Bonding Nanotrap of a Target Molecule through Host−Guest Multiple Hydrogen-Bonding Interactions

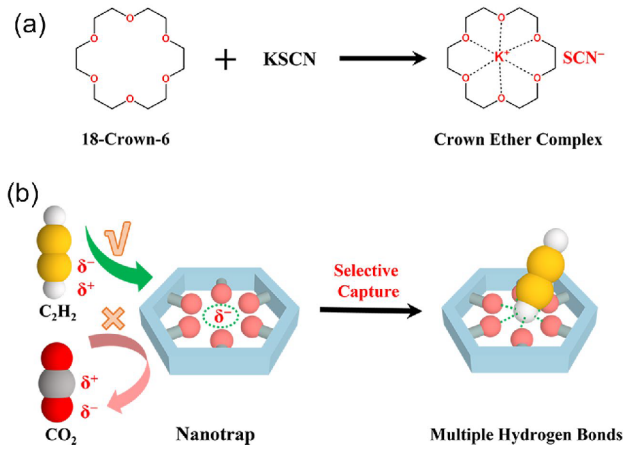

if the hydrogen-bonding nanotrap[51] (as acceptor) is immobilized on the pore surface of porous MOFs, it will not only provide strong hydrogen-bonding interactions to capture acetylene molecules (as donors) but also would not sacrifice the intrinsic pore volume (Scheme 1b).

In this regard, MIL-160, first reported by Serre and co-workers,[52] containing high-density hydrogen-bonding nanotraps within the pore surfaces, could be a promising candidate to achieve the aforementioned mission. To further demonstrate our strategy, here we synthesized three isostructural aluminum-based MOFs (named MIL-160, CAU-10H, and CAU-23, respectively)[52−54] on the basis of the isoreticular features of MOF chemistry and explored their binding abilities for C_2H_2 and C_2H_2/CO_2 separation selectivity for comparison. As expected, MIL-160 with the highest density hydrogen-bonding nanotraps has an excellent C_2H_2 storage capacity (191 cm^3 g^{-1}, or 213 cm^3 cm^{-3}) but a much lower uptake of CO_2 (90 cm^3 g^{-1}) at 298 K and 100 kPa. Notably, the separation performance (storage capacity and selectivity) for C_2H_2/CO_2 mixtures in MIL-160 is significantly higher than that of CAU-10H and CAU-23. Meanwhile, the simulation and experimental breakthroughs have fully demonstrated MIL-160 to be the best porous adsorbent reported thus far for equimolar C_2H_2/CO_2 separation with regard to the separation potential (Δq_{break} = 5.02 mol/kg) and C_2H_2 productivity (6.8 mol/kg). Moreover, computational modeling studies and *in situ* FT-IR tests both reveal that the ultrahigh acetylene storage capacity and superior C_2H_2/CO_2 selectivity of MIL-160 can be mainly attributed to the unique host−guest multiple interactions between the hydrogen-bonding nanotrap and C_2H_2 molecule. This research provides a novel perspective to address the tradeoff for this challenging gas separation.

RESULTS AND DISCUSSION

In these three isostructural MOFs MIL-160, CAU-10H, and CAU-23, each Al(III) atom is coordinated by six O atoms from two hydroxyl and four carboxylate groups, respectively, with a typical AlO_6 octahedral geometry. Notably, in MIL-160 and CAU-10H, the two hydroxyl groups lie in *cis* positions, bridge the adjacent Al centers through a vertex-sharing mode, and form a 1D helical chain secondary building unit (SBU) along the *c* axis (Figure 1, top left). In contrast, another type of 1D

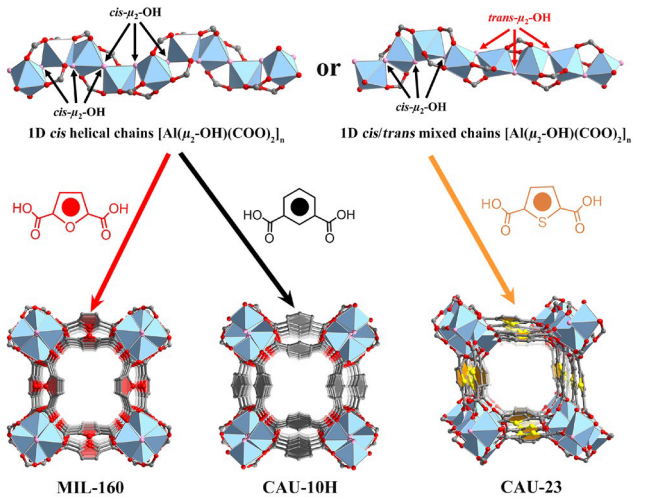

Figure 1. 1D chains $[Al(\mu_2\text{-}OH)(COO)_2]_n$ and V-shaped ligands (H_2FDC, m-H_2BDC, and H_2TDC) assemble into three isostructural 3D frameworks of MIL-160, CAU-10H, and CAU-23, respectively. Hydrogen atoms are omitted for clarity. Color code, Al: pale blue; O, red and rose; C, 50% gray.

chain SBU in CAU-23 is formed by four consecutive alternating units of *trans* and *cis* corner-sharing AlO_6 octahedra; this constructs a novel straight and helical mixed chain (Figure 1, top right). The above two types of 1D chains are quite different from the linear 1D chain with *trans*-connected mode in MIL-53 series of MOFs.[55] These 1D chains are further linked to four adjacent chains by the V-shaped ligands (FDC, m-BDC, and TDC) and extended into a three- dimensional (3D) open framework of MIL-160, CAU-10H, and CAU-23, respectively. After removal of the guest molecules, these three isostructural MOFs exhibit one-dimensional (1D) square channels, with pore aperture sizes of 4.6 × 9.8, 3.6 × 9.2, and 6.3 × 7.6 Å^2, respectively (Figures S3−S5). Furthermore, some basic characteristics (e.g., FT-IR, TGA, and PXRD) of these three MOFs are provided in Figures S6−S14 (see the Supporting Information for details).

The permanent porous behaviors of these three MOFs were first investigated at 77 K with N_2 adsorption experiments. All of them exhibit a fully reversible type I adsorption behavior, with Brunauer−Emmett−Teller (BET) surface areas of 1138, 680, and 1320 m^2 g^{-1} for MIL-160, CAU-10H, and CAU-23, respectively (Figures S15−S17), which are consistent with the previously reported values.[52−54] In addition, the pore-size distributions (PSD) of these three MOFs were analyzed by employing the 77 K N_2 isotherms according to the Horvath−

https://doi.org/10.1021/jacs.1c10620
J. Am. Chem. Soc. 2022, 144, 1681−1689

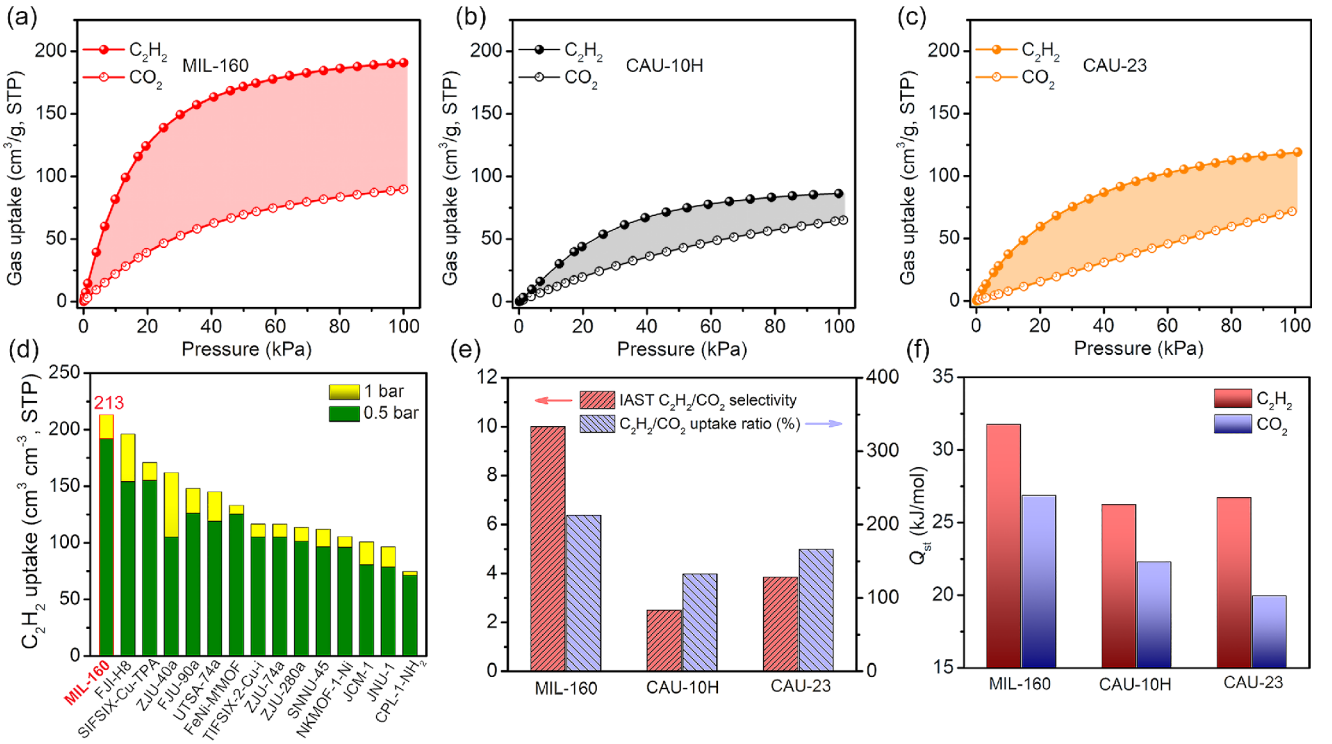

Figure 2. (a–c) Single-component C_2H_2 and CO_2 adsorption isotherms of MIL-160, CAU-10H, and CAU-23, respectivley, at 298 K under 100 kPa. (d) C_2H_2 volumetric uptake of MIL-160 in comparison to other best-performing MOF materials for C_2H_2/CO_2 separation at room temperature. (e) Comparison of C_2H_2/CO_2 selectivity and uptake ratio among these three MOFs at 298 K and 100 kPa. (f) Comparison of the heat of adsorption (Q_{st}) of C_2H_2 and CO_2 at near-zero coverage for MIL-160, CAU-10H, and CAU-23.

Kawazoe cylinder model. All of them display narrow pore size distributions with main peaks at 7.0, 6.0, and 6.8 Å, respectively (Figure S18), consistent with the pore size determined by the crystal structure.

The permanent porosity and suitable pore size of these three MOFs provide us the initial motivation to explore their adsorption behaviors toward C_2H_2 and CO_2. Therefore, the adsorption isotherms of C_2H_2 and CO_2 were collected at 273 and 298 K under 100 kPa pressure. As shown in Figure 2a–c, the C_2H_2 uptake values at 298 K and 100 kPa are 191, 86, and 119 cm^3 g^{-1} for MIL-160, CAU-10H, and CAU-23, respectively. Notably, the gravimetric C_2H_2 uptake value (191 cm^3 g^{-1}) of MIL-160 is remarkably higher than those of the other two isostructural MOFs and is also superior to those of most of the top-performing materials for C_2H_2/CO_2 separation, such as SIFSIX-Cu-TPA (185 cm^3 g^{-1}),[56] FJU-90a (180 cm^3 g^{-1}),[57] UTSA-74a (108 cm^3 g^{-1}),[58] FeNi-M′MOF (96 cm^3 g^{-1}),[59] Cu@FAU (79.5 cm^3 g^{-1}),[60] and Cu^I@UiO-66-$(COOH)_2$ (52 cm^3 g^{-1})[42] and is only lower than that of the benchmark material FJI-H8 (224 cm^3 g^{-1}),[61] which has high-density open Cu sites under similar conditions (Table S6). In the actual separation process, the role of the volumetric storage capacity is even more important than the corresponding gravimetric capacity because it can make full use of the fixed-bed space and minimize the cost of energy regeneration. Under ambient conditions, MIL-160 exhibits the second highest volumetric C_2H_2 adsorption capacity among the reported porous materials with a value of 213 cm^3 cm^{-3}. This value is only slightly lower than the record of 230 cm^3 cm^{-3} for CoMOF-74 with high-density OMS[62] and is significantly higher than those of other best-performing C_2H_2/CO_2 separation materials (e.g., 196 cm^3 cm^{-3} for FJI-H8,[61] 147 cm^3 cm^{-3} for FJU-90a,[57] and 145 cm^3 cm^{-3} for UTSA-74a;[58] Figure 2d) under similar conditions. For equimolar C_2H_2/CO_2 separation, the uptake value of C_2H_2 at a partial pressure of 0.5 bar is another key indicator that needs to be considered. In this regard, the C_2H_2 volumetric uptake of MIL-160 reaches up to 192 cm^3 cm^{-3} (7.7 mmol g^{-1}) at 298 K and 0.5 bar and is also superior to most of the best-performing materials for this separation (Figure 2d).

In addition, the density of the adsorbed acetylene in the channels can be determined as 518, 341, and 262 g/L for MIL-160, CAU-10H, and CAU-23 at 298 K and 100 kPa, respectively, on the basis of their C_2H_2 adsorption capacities and corresponding pore volumes (Table S6). The packing density of C_2H_2 in MIL-160 is notably higher than those of the other two isostructural MOFs and is also about 440 times the density of gaseous C_2H_2 (1.1772 g/L, at 273 K and 101.3 kPa) and is close to the density of solid C_2H_2 at 189 K (729 g/L),[63] indicating that the acetylene molecules can be efficiently packed in the channels of MIL-160. On the other hand, MIL-160 shows the second highest safe acetylene storage density (0.247 g cm^{-3}, slightly lower than the record of 0.267 g cm^{-3} for CoMOF-74; Table S6) in bulk material at 298 K and 100 kPa, which is about 100 times higher than the safe compression limit (0.2 MPa = 0.0021 g cm^{-3}) of C_2H_2 at room temperature.[8] For the practical application of acetylene storage, a promising adsorbent should have good repeatability and structural stability. Thus, we carried out five consecutive acetylene adsorption–desorption isotherm tests. As expected, there was no loss of C_2H_2 storage capacity in MIL-160 after five cycles at 298 K, indicating that MIL-160 is a promising material in refillable C_2H_2 storage (Figure S39).

https://doi.org/10.1021/jacs.1c10620
J. Am. Chem. Soc. 2022, 144, 1681–1689

In contrast, the CO_2 uptake capacities of MIL-160, CAU-10H, and CAU-23 are only 90, 65, and 72 $cm^3\ g^{-1}$, giving C_2H_2/CO_2 uptake ratios of 210%, 130%, and 160% (Figure 2e), respectively, at 100 kPa and 298 K. To further assess the separation performance of MIL-160, CAU-10H, and CAU-23 toward C_2H_2/CO_2 mixtures, the separation selectivity was calculated by using the widely studied ideal adsorbed solution theory (IAST).[64] As shown in Figure S37b, the IAST selectivity of MIL-160 for equimolar C_2H_2/CO_2 mixtures is up to 10 at 298 K and 100 kPa, which is about 2.6 and 4.0 times higher than the corresponding values in CAU-23 (3.8) and CAU-10H (2.5) and higher than those of some of the benchmark porous MOF materials, such as UTSA-74a (8.2),[58] FJU-90a (4.3),[57] MUF-17 (6.0),[65] SIFSIX-21-Ni (7.8),[66] and TIFSIX-2-Cu-i (6.5)[67] under similar conditions. Although some porous materials feature relatively higher C_2H_2/CO_2 selectivity, their adsorption capacity of C_2H_2 is relatively low (usually less than 100 $cm^3\ g^{-1}$ under ambient conditions).[42,43,68] The high uptake ratio and IAST selectivity both suggested the potential of MIL-160 for effective C_2H_2/CO_2 separation.

The affinity between the host framework and the guest molecule can be evaluated by the low-coverage heat of adsorption (Q_{st}). The coverage-dependent Q_{st} values of MIL-160, CAU-10H, and CAU-23 for C_2H_2 and CO_2 were obtained by fitting the single-component gas isotherms collected at 273 and 298 K. As shown in Figure 2f, the near-zero coverage Q_{st} value of C_2H_2 (31.8, 26.2, and 26.7 kJ mol^{-1} for MIL-160, CAU-10H, and CAU-23, respectively) in these three isostructural MOFs is obviously higher than their corresponding values of CO_2 (26.9, 22.3, and 20.0 kJ mol^{-1}), indicating that these MOFs have a stronger affinity for C_2H_2 over CO_2. Unlike CAU-23, the Q_{st} value of C_2H_2 in MIL-160 and CAU-10H gradually increases with an increase in C_2H_2 loading (Figures S21, S24, and S27). This implies that C_2H_2 molecules may form intermolecular interactions during the adsorption process,[69−72] which is consistent with the results of high-density C_2H_2 storage in MIL-160 and CAU-10H. Additionally, the Q_{st} value of C_2H_2 in MIL-160 is lower than those of some benchmark porous materials with high density of OMS, such as Cu-ATC (79.1 kJ mol^{-1}),[10] ZJU-74a (45 kJ mol^{-1}),[73] Cu^I@UiO-66-$(COOH)_2$ (74.5 kJ mol^{-1}),[42] and Cu@FAU (50.0 kJ mol^{-1}).[60] The moderate Q_{st} value of C_2H_2 indicates that MIL-160 can be regenerated under mild conditions, which give it a great potential for energy-efficient C_2H_2/CO_2 separation.

To accurately evaluate the separation performance of porous materials in a fixed bed, we must consider not only the separation selectivity but also the adsorption capacity. To resolve this dilemma, a combined metric, termed the separation potential (Δq), was defined by Krishna.[74,75] Subsequently, transient breakthrough simulations were performed for binary 50/50 or 90/10 C_2H_2/CO_2 mixtures in these three MOFs (Figure S40), operating at a total pressure of 100 kPa and 298 K, by employing the previously reported methodology.[57,74−76] As shown in Figure 3a, the equimolar C_2H_2/CO_2 mixtures can be effectively separated by MIL-160, accompanied by the highest retention time ($\Delta\tau$ = 304; Table S2). Moreover, we compared the two types of separation potential (Δq_{break} and Δq_{IAST}) of MIL-160 with those of other top-performing porous materials for C_2H_2/CO_2 separation under ambient conditions (Figure 3b and Table S2).[57−59,73,77] It is worth noting that MIL-160 has not only the highest Δq_{IAST} (calculated on the basis of the static adsorption isotherms) value of 6.0 mol/kg for equimolar C_2H_2/CO_2 mixtures but also the highest Δq_{break} (5.02 mol/kg, calculated on the basis of the transient breakthrough simulations) value, indicating that MIL-160 has the best separation ability for this gas mixture. In addition, the separation potentials Δq_{break} and Δq_{IAST} have a good positive linear relationship (R^2 = 0.996), with the equation $y = 0.82x + 0.12$. The linear range of this equation is approximately twice that of previously reported results.[77,78] Therefore, this empirical equation can be used to predict porous materials for challenging C_2H_2/CO_2 separation after their Δq_{IAST} values have been calculated.

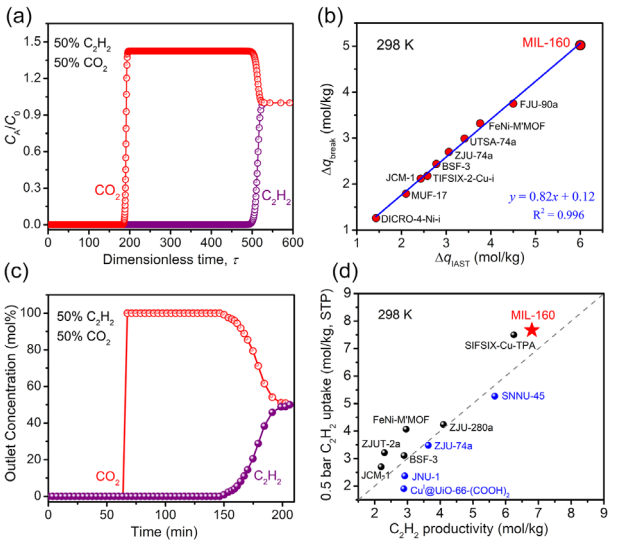

Figure 3. (a) Transient breakthrough curves of equimolar C_2H_2/CO_2 mixtures for MIL-160 at 298 K and 100 kPa. (b) Comparison of the separation potential Δq of MIL-160 with those other benchmark porous materials. Note: the separation potentials Δq_{break} and Δq_{IAST} were calculated on the basis of the transient breakthrough simulations and the static adsorption isotherms for C_2H_2/CO_2 (50/50) mixtures. (c) Experimental breakthrough curves for C_2H_2/CO_2 (50/50) gas mixtures in a laboratory-scale fixed-bed packing with a MIL-160 sample under ambient conditions (298 K, 1 bar). (d) Single-component static C_2H_2 uptake at a partial pressure of 0.5 bar and dynamic C_2H_2 capture amount of equimolar C_2H_2/CO_2 mixtures by MIL-160 in comparison with those of top-performing porous materials at room temperature (black balls, the dotted line, and blue balls indicate that 0.5 bar C_2H_2 uptake is larger than, equal to, and less than dynamic C_2H_2 capture, respectively).

The record-high separation potential prompted us to evaluate the separation performance of MIL-160 for challenging C_2H_2/CO_2 mixtures under real conditions. We performed laboratory-scale dynamic breakthrough experiments, with the equimolar C_2H_2/CO_2 mixtures being flowed through a packed column filled with an activated sample (~1.2 g) at a total flow rate of 2 mL min^{-1} under ambient conditions. As shown in Figure 3c, the C_2H_2/CO_2 mixture can be efficiently separated, in which the CO_2 is eluted first at 64 min and rapidly reaches up to a pure grade without acetylene outflow, and this process continued for ~86 min, a remarkable time to obtain pure CO_2, until the saturated uptake of acetylene and thus breakthrough (at 150 min). According to the breakthrough curve, the dynamic C_2H_2 capture amount (also named productivity) was found to be 6.8 mol/kg for a given cycle, which is highly consistent with the equilibrium adsorption of C_2H_2 under similar conditions (7.7 mol/kg, at 298 K and 0.5 bar). Notably, the dynamic C_2H_2 productivity of

https://doi.org/10.1021/jacs.1c10620
J. Am. Chem. Soc. 2022, 144, 1681−1689

MIL-160 is among the highest values achieved and is much higher than those of most benchmark porous materials (Figure 3d, Table S3), such as FeNi-M′MOF (2.96 mol/kg),[59] ZJU-74a (3.64 mol/kg),[73] and Cu^{I}@UiO-66-$(COOH)_2$ (2.89 mol/kg).[42] Therefore, MIL-160 establishes a new benchmark for the separation of challenging C_2H_2/CO_2 mixtures under actual conditions. Considering the need for recyclability in industrial applications, we carried out a multicycle mixed-gas breakthrough experiment under the same conditions. The results indicate no notable loss in the breakthrough time and C_2H_2 capture capacity of MIL-160 in four consecutive cycles (Figures S41−S43), which proves that it maintains excellent repeatability for C_2H_2/CO_2 separation.

In situ infrared (IR) spectroscopic measurements were conducted to further probe the interaction of C_2H_2 within three MOF structures: namely, MIL-160, CAU-23, and CAU-10H. C_2H_2 is well-known to have an acidic nature and thus tends to form hydrogen bonds within the basic sites, as observed in several MOFs.[34,79,80] Similar to the well-studied OH stretching vibration,[81] the $\nu_{as}(C_2H_2)$ band undergoes a downward shift with reference to the gas-phase value at 3287 cm^{-1} when it is subjected to a hydrogen-bonding interaction and the frequency shift is a measure of intermolecular H bonds. Figure 4 presents the stretching band of adsorbed

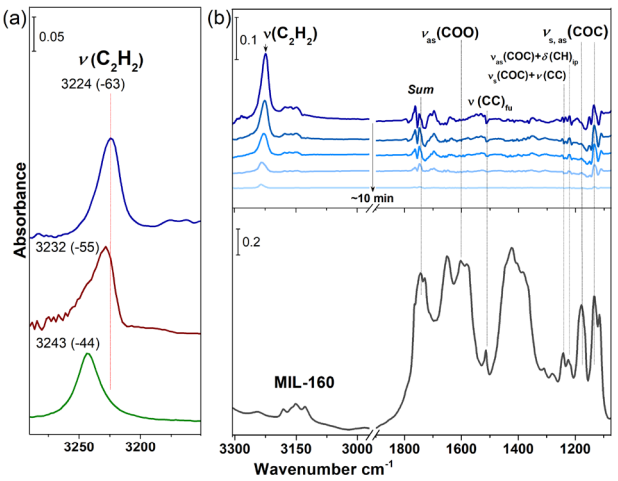

Figure 4. (a) IR spectra showing the stretching band of adsorbed C_2H_2 inside MIL-160 (blue), CAU-23 (brown), and CAU-10 (green) upon loading C_2H_2 gas at ∼400 Torr (see full spectra in Figure 4b and Figure S45). The signal of gas-phase C_2H_2 is subtracted. The values in parentheses show the shift of the $\nu_{as}(C_2H_2)$ band with respect to the gas phase at 3287 cm^{-1}. (b) The top five difference spectra showing the unloading of C_2H_2 from MIL-160 upon evacuation of the gas phase for ∼10 min; each is referenced to the bottom spectrum of activated MIL-160 under vacuum. Notation and acronyms: ν, stretch; δ, deformation; as, asymmetric; s, symmetric; ip, in plane; sum, summation band; fu, furan ring.

acetylene upon loading C_2H_2 at ∼400 Torr into three MOFs and its desorption from MIL-160 after evacuating the gas phase. As shown in Figure 4a, $\nu_{as}(C_2H_2)$ bands occur at 3224, 3232, and 3243 cm^{-1} in MIL-160, CAU-23, and CAU-10H, respectively. The trend of band position shift indicates that hydrogen-bonding interactions follow the order MIL-160 > CAU-23 > CAU-10H. In addition, different spectra shown in Figure 4b show that vibrational modes associated with the organic linker, including the COC symmetric and asymmetric stretch at 1178 and 1133 cm^{-1}, the coupled COC stretch/CC stretch/in-plane C−H deformation at 1242−1224 cm^{-1}, the furan ring carbon stretch at 1514 cm^{-1}, the carboxylate asymmetric stretch at 1580−1602 cm^{-1},[82] and the out-of-plane C−H summation band at 1743 cm^{-1},[83] are appreciably perturbed upon loading acetylene into MIL-160 (see assignment in Table S4). With desorption of the trapped acetylene from MIL-160, the perturbations of these modes gradually disappeared, as seen in Figure 4b. These observations point to the direct interaction of loaded C_2H_2 molecules with both COO- and the O-containing ring of the FDC linker, as further verified by our modeling studies (Table S4).

To gain insight into the binding sites of C_2H_2 and CO_2 in MIL-160, modeling studies based on simulated annealing calculations and canonical Monte Carlo (CMC) simulations were performed (see the Supporting Information for details). As shown in Figure S46, three and two possible binding sites of C_2H_2 and CO_2 were found in MIL-160, respectively. Here, we focus on discussing and comparing the primary binding site of C_2H_2 and CO_2 in MIL-160, and discussions on other binding sites are provided in the Supporting Information. It was observed that the orientation of the C_2H_2 (I) molecule is roughly perpendicular to the MOF channel (Figure S46a), where it forms multiple $H-C\equiv C-H^{\delta+}\cdots O^{\delta-}$ hydrogen-bonding interactions with the nearby carboxylate groups and furan rings, forming a nanotrap on the pore surface, with close interaction distances ranging from 2.51 to 3.57 Å (Figure 5a).

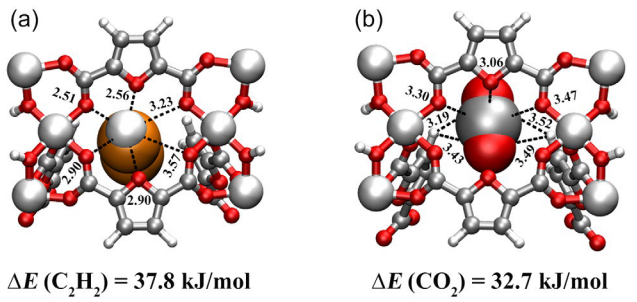

Figure 5. Canonical Monte Carlo (CMC) simulated primary binding sites of (a) C_2H_2 and (b) CO_2 in MIL-160. Distances are given in Å.

In contrast, the CO_2 (I) molecule is oriented parallel to the *c* axis in the channels (Figure S46b),[84] in which $(CO_2)C^{\delta+}\cdots O^{\delta-}$ electrostatic interactions with the carboxylate groups and the furan O atom (distances ranging from 3.06 to 3.47 Å) and $CH^{\delta+}\cdots O^{\delta-}(CO_2)$ interactions with the nearby furan rings (distances ranging from 3.19 to 3.52 Å) were observed (Figure 5b). Overall, C_2H_2 exhibits typically shorter interaction distances with MIL-160 at the primary binding site in comparison to CO_2, which accounts for the stronger affinity of C_2H_2 with the adsorbent. The calculated binding energies (37.8 vs 32.7 kJ mol^{-1}) for single C_2H_2 and CO_2 molecules positioned at their global minimum in MIL-160 from CMC simulations were consistent with the trend in the experimental low-coverage Q_{st} values (31.8 vs 26.9 kJ mol^{-1}) from single-component adsorption isotherms (Table S5). In summary, the binding configurations in MIL-160 calculated herein combine key features that cause stronger C_2H_2 binding versus CO_2: multiple $H-C\equiv C-H^{\delta+}\cdots O^{\delta-}$ hydrogen-bonding interactions and weak CO_2−sorbent electrostatic interactions.

The diffusion of C_2H_2 and CO_2 molecules inside MIL-160 was investigated by looking at various transition-state configurations of the molecules traveling through the MOF

https://doi.org/10.1021/jacs.1c10620
J. Am. Chem. Soc. 2022, 144, 1681−1689

channel using the climbing nudged elastic band (cNEB) method.[85,86] To better understand the interaction taking place during molecular diffusion, induced charge densities were mapped for the initial, transition, and final states, as shown in Figure S48. For the initial configuration (at 0% progress), both C_2H_2 and CO_2 molecules occupy the space near their respective primary binding sites, giving the lowest energy to this configuration. Subsequently, the gas molecules move along the channel, getting to the highest energy configuration with diffusion barriers of 157 meV for C_2H_2 and 161 meV for CO_2, respectively. At the initial state, C_2H_2 and CO_2 show interactions with the MOF linkers, as evidenced by the yellow/blue induced charge densities in Figure S48. However, at the transition configuration CO_2 shows a reduced interaction with the surrounding linkers, as evidenced by the reduction in induced charge density. In contrast, C_2H_2 still exhibits strong interaction with the linker atoms (see Figure S48a for the transition state). This results in a transition configuration that is more stable for C_2H_2 in comparison to CO_2. Therefore, the diffusion energy barrier of C_2H_2 is slightly lower, leading to a faster molecular transport along the MOF channel, indicating that less energy is required for acetylene molecules to leave the strong binding site and diffuse along the MOF channel. The higher binding energy and lower diffusion kinetic barrier well explain the high separation selectivity of C_2H_2/CO_2 in MIL-160.

CONCLUSIONS

To conclude, we have successfully demonstrated that the high-density hydrogen-bonding nanotrap within the pore surface of porous MOFs can achieve highly selective C_2H_2/CO_2 separation. By virtue of the isoreticular principle in MOF chemistry, we can fine-tune the hydrogen-bonding acceptors on the pore surface, as illustrated in three isostructural MOFs. Notably, MIL-160 features the highest density of hydrogen-bonding nanotraps and exhibits a high acetylene storage capacity and superior separation selectivity simultaneously, supplying a new benchmark for C_2H_2/CO_2 separation with an excellent separation potential and high C_2H_2 productivity under ambient conditions. This research provides an outstanding example of a MOF-based hydrogen-bonding nanotrap to address this challenge of gas separation/purification and thus provides a new perspective for rationally designing porous MOF materials in this very active research area.

ASSOCIATED CONTENT

Supporting Information

The Supporting Information is available free of charge at https://pubs.acs.org/doi/10.1021/jacs.1c10620.

Material synthesis, characterization details, and additional figures as described in the text (PDF)

AUTHOR INFORMATION

Corresponding Authors

Jing Li − *Department of Chemistry and Chemical Biology, Rutgers University, Piscataway, New Jersey 08854, United States;* orcid.org/0000-0001-7792-4322; Email: jingli@rutgers.edu

Shengqian Ma − *Department of Chemistry, University of North Texas, Denton, Texas 76201, United States;* orcid.org/0000-0002-1897-7069; Email: Shengqian.Ma@unt.edu

Authors

Yingxiang Ye − *Department of Chemistry, University of North Texas, Denton, Texas 76201, United States;* orcid.org/0000-0003-3962-8463

Shikai Xian − *Department of Chemistry and Chemical Biology, Rutgers University, Piscataway, New Jersey 08854, United States; Hoffmann Institute of Advanced Materials, Shenzhen Polytechnic, Shenzhen, Guangdong 518055, People's Republic of China*

Hui Cui − *Department of Chemistry, University of Texas at San Antonio, San Antonio, Texas 78249-0698, United States;* orcid.org/0000-0002-9723-4932

Kui Tan − *Department of Materials Science & Engineering, University of Texas at Dallas, Richardson, Texas 75080, United States;* orcid.org/0000-0002-5167-7295

Lingshan Gong − *Department of Chemistry, University of North Texas, Denton, Texas 76201, United States*

Bin Liang − *Department of Chemistry, University of North Texas, Denton, Texas 76201, United States*

Tony Pham − *Department of Chemistry, University of South Florida, Tampa, Florida 33620, United States;* orcid.org/0000-0001-5654-163X

Haardik Pandey − *Department of Physics and Center for Functional Materials, Wake Forest University, Winston-Salem, North Carolina 27109, United States*

Rajamani Krishna − *Van 't Hoff Institute for Molecular Sciences, University of Amsterdam, 1098 XH Amsterdam, The Netherlands;* orcid.org/0000-0002-4784-8530

Pui Ching Lan − *Department of Chemistry, University of North Texas, Denton, Texas 76201, United States*

Katherine A. Forrest − *Department of Chemistry, University of South Florida, Tampa, Florida 33620, United States*

Brian Space − *Department of Chemistry, North Carolina State University, Raleigh, North Carolina 27695, United States*

Timo Thonhauser − *Department of Physics and Center for Functional Materials, Wake Forest University, Winston-Salem, North Carolina 27109, United States;* orcid.org/0000-0003-4771-7511

Complete contact information is available at: https://pubs.acs.org/10.1021/jacs.1c10620

Author Contributions

●Y.Y. and S.X. contributed equally to this work.

Notes

The authors declare no competing financial interest.

ACKNOWLEDGMENTS

We acknowledge the Robert A. Welch Foundation (B-0027) and the U.S. National Science Foundation (ECCS- 2029800) for financial support of this work. We also extend our sincere appreciation to the U.S. Department of Energy, Office of Science, Office of Basic Energy Sciences, under Award DE-SC0019902. T.P., K.A.F., and B.S. acknowledge the National Science Foundation (Award No. DMR-1607989), including support from the Major Research Instrumentation Program (Award No. CHE-1531590). Computational resources were made available by a XSEDE Grant (No. TG-DMR090028) and by Research Computing at the University of South Florida. Adam Hogan is also acknowledged for calculating the polarizability for Al^{3+}.

REFERENCES

(1) Li, J. R.; Kuppler, R. J.; Zhou, H. C. Selective gas adsorption and separation in metal-organic frameworks. *Chem. Soc. Rev.* **2009**, *38*, 1477−1504.

(2) Lin, R.-B.; Xiang, S.; Zhou, W.; Chen, B. Microporous Metal-Organic Framework Materials for Gas Separation. *Chem* **2020**, *6*, 337−363.

(3) Wu, Y.; Weckhuysen, B. M. Separation and Purification of Hydrocarbons with Porous Materials. *Angew. Chem., Int. Ed.* **2021**, *60*, 18930−18949.

(4) Yang, Y.; Li, L.; Lin, R. B.; Ye, Y.; Yao, Z.; Yang, L.; Xiang, F.; Chen, S.; Zhang, Z.; Xiang, S.; Chen, B. Ethylene/ethane separation in a stable hydrogen-bonded organic framework through a gating mechanism. *Nat. Chem.* **2021**, *13*, 933−939.

(5) Stang, P. J.; Diederich, F. *Modern acetylene chemistry*; VCH: 1995.

(6) Guo, C. J.; Shen, D.; Bülow, M. 18-O-03 - Kinetic separation of binary mixtures of carbon dioxide and C_2 hydrocarbons on modified LTA-type zeolites. *Stud. Surf. Sci. Catal.* **2001**, *135*, 144.

(7) Reid, C. R.; Thomas, K. M. Adsorption Kinetics and Size Exclusion Properties of Probe Molecules for the Selective Porosity in a Carbon Molecular Sieve Used for Air Separation. *J. Phys. Chem. B* **2001**, *105*, 10619−10629.

(8) Matsuda, R.; Kitaura, R.; Kitagawa, S.; Kubota, Y.; Belosludov, R. V.; Kobayashi, T. C.; Sakamoto, H.; Chiba, T.; Takata, M.; Kawazoe, Y.; Mita, Y. Highly controlled acetylene accommodation in a metal−organic microporous material. *Nature* **2005**, *436*, 238−241.

(9) Ye, Y.; Chen, S.; Chen, L.; Huang, J.; Ma, Z.; Li, Z.; Yao, Z.; Zhang, J.; Zhang, Z.; Xiang, S. Additive-Induced Supramolecular Isomerism and Enhancement of Robustness in Co(II)-Based MOFs for Efficiently Trapping Acetylene from Acetylene-Containing Mixtures. *ACS Appl. Mater. Interfaces* **2018**, *10*, 30912−30918.

(10) Niu, Z.; Cui, X.; Pham, T.; Verma, G.; Lan, P. C.; Shan, C.; Xing, H.; Forrest, K. A.; Suepaul, S.; Space, B.; Nafady, A.; Al-Enizi, A. M.; Ma, S. A MOF-based Ultra-Strong Acetylene Nano-trap for Highly Efficient C_2H_2/CO_2 Separation. *Angew. Chem., Int. Ed.* **2021**, *60*, 5283−5288.

(11) Chu, S.; Cui, Y.; Liu, N. The path towards sustainable energy. *Nat. Mater.* **2017**, *16*, 16−22.

(12) Sircar, S. Pressure Swing Adsorption. *Ind. Eng. Chem. Res.* **2002**, *41*, 1389−1392.

(13) Mason, J. A.; Sumida, K.; Herm, Z. R.; Krishna, R.; Long, J. R. Evaluating metal−organic frameworks for post-combustion carbon dioxide capture via temperature swing adsorption. *Energy Environ. Sci.* **2011**, *4*, 3030−3040.

(14) Ye, Y.; Ma, Z.; Chen, L.; Lin, H.; Lin, Q.; Liu, L.; Li, Z.; Chen, S.; Zhang, Z.; Xiang, S. Microporous metal−organic frameworks with open metal sites and π-Lewis acidic pore surfaces for recovering ethylene from polyethylene off-gas. *J. Mater. Chem. A* **2018**, *6*, 20822−20828.

(15) Qian, Q.; Asinger, P. A.; Lee, M. J.; Han, G.; Mizrahi Rodriguez, K.; Lin, S.; Benedetti, F. M.; Wu, A. X.; Chi, W. S.; Smith, Z. P. MOF-Based Membranes for Gas Separations. *Chem. Rev.* **2020**, *120*, 8161−8266.

(16) Sholl, D. S.; Lively, R. P. Seven chemical separations to change the world. *Nature* **2016**, *532*, 435−437.

(17) Furukawa, H.; Cordova, K. E.; O'Keeffe, M.; Yaghi, O. M. The chemistry and applications of metal-organic frameworks. *Science* **2013**, *341*, 1230444.

(18) Zhao, X.; Wang, Y.; Li, D. S.; Bu, X.; Feng, P. Metal-Organic Frameworks for Separation. *Adv. Mater.* **2018**, *30*, 1705189.

(19) Li, H.; Li, L.; Lin, R.-B.; Zhou, W.; Zhang, Z.; Xiang, S.; Chen, B. Porous metal-organic frameworks for gas storage and separation: Status and challenges. *EnergyChem* **2019**, *1*, 100006.

(20) Wang, H.; Liu, Y.; Li, J. Designer Metal-Organic Frameworks for Size-Exclusion-Based Hydrocarbon Separations: Progress and Challenges. *Adv. Mater.* **2020**, *32*, 2002603.

(21) Ye, Y.; Gong, L.; Xiang, S.; Zhang, Z.; Chen, B. Metal-Organic Frameworks as a Versatile Platform for Proton Conductors. *Adv. Mater.* **2020**, *32*, 1907090.

(22) Vaidhyanathan, R.; Iremonger, S. S.; Shimizu, G. K.; Boyd, P. G.; Alavi, S.; Woo, T. K. Direct observation and quantification of CO_2 binding within an amine-functionalized nanoporous solid. *Science* **2010**, *330*, 650−653.

(23) Lin, R. B.; Zhang, Z.; Chen, B. Achieving High Performance Metal-Organic Framework Materials through Pore Engineering. *Acc. Chem. Res.* **2021**, *54*, 3362−3376.

(24) Bereciartua, P. J.; Cantin, A.; Corma, A.; Jorda, J. L.; Palomino, M.; Rey, F.; Valencia, S.; Corcoran, E. W., Jr.; Kortunov, P.; Ravikovitch, P. I.; Burton, A.; Yoon, C.; Wang, Y.; Paur, C.; Guzman, J.; Bishop, A. R.; Casty, G. L. Control of zeolite framework flexibility and pore topology for separation of ethane and ethylene. *Science* **2017**, *358*, 1068−1071.

(25) Sevilla, M.; Fuertes, A. B. Sustainable porous carbons with a superior performance for CO_2 capture. *Energy Environ. Sci.* **2011**, *4*, 1765−1771.

(26) Chen, Z.; Li, P.; Anderson, R.; Wang, X.; Zhang, X.; Robison, L.; Redfern, L. R.; Moribe, S.; Islamoglu, T.; Gomez-Gualdron, D. A.; Yildirim, T.; Stoddart, J. F.; Farha, O. K. Balancing volumetric and gravimetric uptake in highly porous materials for clean energy. *Science* **2020**, *368*, 297−303.

(27) Chen, Z.; Jiang, H.; Li, M.; O'Keeffe, M.; Eddaoudi, M. Reticular Chemistry 3.2: Typical Minimal Edge-Transitive Derived and Related Nets for the Design and Synthesis of Metal-Organic Frameworks. *Chem. Rev.* **2020**, *120*, 8039−8065.

(28) Kim, E. J.; Siegelman, R. L.; Jiang, H. Z. H.; Forse, A. C.; Lee, J.-H.; Martell, J. D.; Milner, P. J.; Falkowski, J. M.; Neaton, J. B.; Reimer, J. A.; Weston, S. C.; Long, J. R. Cooperative carbon capture and steam regeneration with tetraamine-appended metal−organic frameworks. *Science* **2020**, *369*, 392−396.

(29) Liao, P. Q.; Huang, N. Y.; Zhang, W. X.; Zhang, J. P.; Chen, X. M. Controlling guest conformation for efficient purification of butadiene. *Science* **2017**, *356*, 1193−1196.

(30) Li, L.; Lin, R. B.; Krishna, R.; Li, H.; Xiang, S.; Wu, H.; Li, J.; Zhou, W.; Chen, B. Ethane/ethylene separation in a metal-organic framework with iron-peroxo sites. *Science* **2018**, *362*, 443−446.

(31) Lin, R. B.; Li, L.; Zhou, H. L.; Wu, H.; He, C.; Li, S.; Krishna, R.; Li, J.; Zhou, W.; Chen, B. Molecular sieving of ethylene from ethane using a rigid metal-organic framework. *Nat. Mater.* **2018**, *17*, 1128−1133.

(32) Wang, H.; Dong, X.; Colombo, V.; Wang, Q.; Liu, Y.; Liu, W.; Wang, X. L.; Huang, X. Y.; Proserpio, D. M.; Sironi, A.; Han, Y.; Li, J. Tailor-Made Microporous Metal-Organic Frameworks for the Full Separation of Propane from Propylene Through Selective Size Exclusion. *Adv. Mater.* **2018**, *30*, 1805088.

(33) Gu, C.; Hosono, N.; Zheng, J. J.; Sato, Y.; Kusaka, S.; Sakaki, S.; Kitagawa, S. Design and control of gas diffusion process in a nanoporous soft crystal. *Science* **2019**, *363*, 387−391.

(34) Chen, K. J.; Madden, D. G.; Mukherjee, S.; Pham, T.; Forrest, K. A.; Kumar, A.; Space, B.; Kong, J.; Zhang, Q. Y.; Zaworotko, M. J. Synergistic sorbent separation for one-step ethylene purification from a four-component mixture. *Science* **2019**, *366*, 241−246.

(35) Liang, B.; Zhang, X.; Xie, Y.; Lin, R. B.; Krishna, R.; Cui, H.; Li, Z.; Shi, Y.; Wu, H.; Zhou, W.; Chen, B. An Ultramicroporous Metal-Organic Framework for High Sieving Separation of Propylene from Propane. *J. Am. Chem. Soc.* **2020**, *142*, 17795−17801.

(36) Xiang, S.; Zhou, W.; Gallegos, J. M.; Liu, Y.; Chen, B. Exceptionally High Acetylene Uptake in a Microporous Metal−Organic Framework with Open Metal Sites. *J. Am. Chem. Soc.* **2009**, *131*, 12415−12419.

(37) He, Y. B.; Krishna, R.; Chen, B. L. Metal-organic frameworks with potential for energy-efficient adsorptive separation of light hydrocarbons. *Energy Environ. Sci.* **2012**, *5*, 9107−9120.

(38) Moreau, F.; da Silva, I.; Al Smail, N. H.; Easun, T. L.; Savage, M.; Godfrey, H. G.; Parker, S. F.; Manuel, P.; Yang, S.; Schroder, M. Unravelling exceptional acetylene and carbon dioxide adsorption

https://doi.org/10.1021/jacs.1c10620
J. Am. Chem. Soc. 2022, 144, 1681−1689

within a tetra-amide functionalized metal-organic framework. *Nat. Commun.* **2017**, *8*, 14085.
(39) Di, Z.; Liu, C.; Pang, J.; Chen, C.; Hu, F.; Yuan, D.; Wu, M.; Hong, M. Cage-Like Porous Materials with Simultaneous High C_2H_2 Storage and Excellent C_2H_2/CO_2 Separation Performance. *Angew. Chem., Int. Ed.* **2021**, *60*, 10828−10832.
(40) Scott, H. S.; Shivanna, M.; Bajpai, A.; Madden, D. G.; Chen, K. J.; Pham, T.; Forrest, K. A.; Hogan, A.; Space, B.; Perry, J. J., IV; Zaworotko, M. J. Highly Selective Separation of C_2H_2 from CO_2 by a New Dichromate-Based Hybrid Ultramicroporous Material. *ACS Appl. Mater. Interfaces* **2017**, *9*, 33395−33400.
(41) Lin, R. B.; Li, L.; Wu, H.; Arman, H.; Li, B.; Lin, R. G.; Zhou, W.; Chen, B. Optimized Separation of Acetylene from Carbon Dioxide and Ethylene in a Microporous Material. *J. Am. Chem. Soc.* **2017**, *139*, 8022−8028.
(42) Zhang, L.; Jiang, K.; Yang, L.; Li, L.; Hu, E.; Yang, L.; Shao, K.; Xing, H.; Cui, Y.; Yang, Y.; Li, B.; Chen, B.; Qian, G. Benchmark C_2H_2 /CO_2 Separation in an Ultra-Microporous Metal-Organic Framework via Copper(I)-Alkynyl Chemistry. *Angew. Chem., Int. Ed.* **2021**, *60*, 15995−16002.
(43) Yang, L.; Yan, L.; Wang, Y.; Liu, Z.; He, J.; Fu, Q.; Liu, D.; Gu, X.; Dai, P.; Li, L.; Zhao, X. Adsorption Site Selective Occupation Strategy within a Metal-Organic Framework for Highly Efficient Sieving Acetylene from Carbon Dioxide. *Angew. Chem., Int. Ed.* **2021**, *60*, 4570−4574.
(44) Li, B.; Cui, X.; O'Nolan, D.; Wen, H. M.; Jiang, M.; Krishna, R.; Wu, H.; Lin, R. B.; Chen, Y. S.; Yuan, D.; Xing, H.; Zhou, W.; Ren, Q.; Qian, G.; Zaworotko, M. J.; Chen, B. An Ideal Molecular Sieve for Acetylene Removal from Ethylene with Record Selectivity and Productivity. *Adv. Mater.* **2017**, *29*, 1704210.
(45) Chen, K. J.; Madden, D. G.; Pham, T.; Forrest, K. A.; Kumar, A.; Yang, Q. Y.; Xue, W.; Space, B.; Perry, J. J. t.; Zhang, J. P.; Chen, X. M.; Zaworotko, M. J. Tuning Pore Size in Square-Lattice Coordination Networks for Size-Selective Sieving of CO_2. *Angew. Chem., Int. Ed.* **2016**, *55*, 10268−10272.
(46) Graham, C.; Pierrus, J.; Raab, R. E. Measurement of the electric quadrupole moments of CO_2, CO and N_2. *Mol. Phys.* **1989**, *67*, 939−955.
(47) Halkier, A.; Coriani, S. On the molecular electric quadrupole moment of C_2H_2. *Chem. Phys. Lett.* **1999**, *303*, 408−412.
(48) Pedersen, C. J. Cyclic polyethers and their complexes with metal salts. *J. Am. Chem. Soc.* **1967**, *89*, 7017−7036.
(49) Escobar, L.; Ballester, P. Molecular Recognition in Water Using Macrocyclic Synthetic Receptors. *Chem. Rev.* **2021**, *121*, 2445−2514.
(50) Liu, W.; Oliver, A. G.; Smith, B. D. Macrocyclic Receptor for Precious Gold, Platinum, or Palladium Coordination Complexes. *J. Am. Chem. Soc.* **2018**, *140*, 6810−6813.
(51) Yang, L.; Cui, X.; Yang, Q.; Qian, S.; Wu, H.; Bao, Z.; Zhang, Z.; Ren, Q.; Zhou, W.; Chen, B.; Xing, H. A Single-Molecule Propyne Trap: Highly Efficient Removal of Propyne from Propylene with Anion-Pillared Ultramicroporous Materials. *Adv. Mater.* **2018**, *30*, 1705374.
(52) Cadiau, A.; Lee, J. S.; Damasceno Borges, D.; Fabry, P.; Devic, T.; Wharmby, M. T.; Martineau, C.; Foucher, D.; Taulelle, F.; Jun, C. H.; Hwang, Y. K.; Stock, N.; De Lange, M. F.; Kapteijn, F.; Gascon, J.; Maurin, G.; Chang, J. S.; Serre, C. Design of hydrophilic metal organic framework water adsorbents for heat reallocation. *Adv. Mater.* **2015**, *27*, 4775−4780.
(53) Reinsch, H.; van der Veen, M. A.; Gil, B.; Marszalek, B.; Verbiest, T.; de Vos, D.; Stock, N. Structures, Sorption Characteristics, and Nonlinear Optical Properties of a New Series of Highly Stable Aluminum MOFs. *Chem. Mater.* **2013**, *25*, 17−26.
(54) Lenzen, D.; Zhao, J.; Ernst, S. J.; Wahiduzzaman, M.; Ken Inge, A.; Frohlich, D.; Xu, H.; Bart, H. J.; Janiak, C.; Henninger, S.; Maurin, G.; Zou, X.; Stock, N. A metal-organic framework for efficient water-based ultra-low-temperature-driven cooling. *Nat. Commun.* **2019**, *10*, 3025.
(55) Millange, F.; Serre, C.; Ferey, G. Synthesis, structure determination and properties of MIL-53as and MIL-53ht: the first CrIII hybrid inorganic-organic microporous solids: $Cr^{III}(OH).(O_2C\text{-}C_6H_4\text{-}CO_2).(HO_2C\text{-}C_6H_4\text{-}CO_2H)_x$. *Chem. Commun.* **2002**, 822−823.
(56) Li, H.; Liu, C.; Chen, C.; Di, Z.; Yuan, D.; Pang, J.; Wei, W.; Wu, M.; Hong, M. An Unprecedented Pillar-Cage Fluorinated Hybrid Porous Framework with Highly Efficient Acetylene Storage and Separation. *Angew. Chem., Int. Ed.* **2021**, *60*, 7547−7552.
(57) Ye, Y.; Ma, Z.; Lin, R.-B.; Krishna, R.; Zhou, W.; Lin, Q.; Zhang, Z.; Xiang, S.; Chen, B. Pore Space Partition within a Metal−Organic Framework for Highly Efficient C_2H_2/CO_2 Separation. *J. Am. Chem. Soc.* **2019**, *141*, 4130−4136.
(58) Luo, F.; Yan, C.; Dang, L.; Krishna, R.; Zhou, W.; Wu, H.; Dong, X.; Han, Y.; Hu, T. L.; O'Keeffe, M.; Wang, L.; Luo, M.; Lin, R. B.; Chen, B. UTSA-74: A MOF-74 Isomer with Two Accessible Binding Sites per Metal Center for Highly Selective Gas Separation. *J. Am. Chem. Soc.* **2016**, *138*, 5678−5684.
(59) Gao, J.; Qian, X.; Lin, R. B.; Krishna, R.; Wu, H.; Zhou, W.; Chen, B. Mixed Metal-Organic Framework with Multiple Binding Sites for Efficient C_2H_2/CO_2 Separation. *Angew. Chem., Int. Ed.* **2020**, *59*, 4396−4400.
(60) Liu, S.; Han, X.; Chai, Y.; Wu, G.; Li, W.; Li, J.; da Silva, I.; Manuel, P.; Cheng, Y.; Daemen, L. L.; Ramirez-Cuesta, A. J.; Shi, W.; Guan, N.; Yang, S.; Li, L. Efficient Separation of Acetylene and Carbon Dioxide in a Decorated Zeolite. *Angew. Chem., Int. Ed.* **2021**, *60*, 6526−6532.
(61) Pang, J.; Jiang, F.; Wu, M.; Liu, C.; Su, K.; Lu, W.; Yuan, D.; Hong, M. A porous metal-organic framework with ultrahigh acetylene uptake capacity under ambient conditions. *Nat. Commun.* **2015**, *6*, 7575.
(62) Xiang, S.; Zhou, W.; Zhang, Z.; Green, M. A.; Liu, Y.; Chen, B. Open metal sites within isostructural metal-organic frameworks for differential recognition of acetylene and extraordinarily high acetylene storage capacity at room temperature. *Angew. Chem., Int. Ed.* **2010**, *49*, 4615−4618.
(63) McIntosh, D. The Physical Properties of Liquid and Solid Acetylene. *J. Phys. Chem.* **1907**, *11*, 306−317.
(64) Myers, A. L.; Prausnitz, J. M. Thermodynamics of mixed-gas adsorption. *AIChE J.* **1965**, *11*, 121−127.
(65) Qazvini, O. T.; Babarao, R.; Telfer, S. G. Multipurpose Metal−Organic Framework for the Adsorption of Acetylene: Ethylene Purification and Carbon Dioxide Removal. *Chem. Mater.* **2019**, *31*, 4919−4926.
(66) Kumar, N.; Mukherjee, S.; Harvey-Reid, N. C.; Bezrukov, A. A.; Tan, K.; Martins, V.; Vandichel, M.; Pham, T.; van Wyk, L. M.; Oyekan, K.; Kumar, A.; Forrest, K. A.; Patil, K. M.; Barbour, L. J.; Space, B.; Huang, Y.; Kruger, P. E.; Zaworotko, M. J. Breaking the trade-off between selectivity and adsorption capacity for gas separation. *Chem* **2021**, *7*, 3085−3098.
(67) Chen, K. J.; Scott, H. S.; Madden, D. G.; Pham, T.; Kumar, A.; Bajpai, A.; Lusi, M.; Forrest, K. A.; Space, B.; Perry, J. J.; Zaworotko, M. J. Benchmark C_2H_2/CO_2 and CO_2/C_2H_2 Separation by Two Closely Related Hybrid Ultramicroporous Materials. *Chem* **2016**, *1*, 753−765.
(68) Li, P.; He, Y.; Zhao, Y.; Weng, L.; Wang, H.; Krishna, R.; Wu, H.; Zhou, W.; O'Keeffe, M.; Han, Y.; Chen, B. A rod-packing microporous hydrogen-bonded organic framework for highly selective separation of C_2H_2/CO_2 at room temperature. *Angew. Chem., Int. Ed.* **2015**, *54*, 574−577.
(69) Cui, X.; Chen, K.; Xing, H.; Yang, Q.; Krishna, R.; Bao, Z.; Wu, H.; Zhou, W.; Dong, X.; Han, Y.; Li, B.; Ren, Q.; Zaworotko, M. J.; Chen, B. Pore chemistry and size control in hybrid porous materials for acetylene capture from ethylene. *Science* **2016**, *353*, 141−144.
(70) Gong, W.; Cui, H.; Xie, Y.; Li, Y.; Tang, X.; Liu, Y.; Cui, Y.; Chen, B. Efficient C_2H_2/CO_2 Separation in Ultramicroporous Metal-Organic Frameworks with Record C_2H_2 Storage Density. *J. Am. Chem. Soc.* **2021**, *143*, 14869−14876.
(71) Yang, S.; Ramirez-Cuesta, A. J.; Newby, R.; Garcia-Sakai, V.; Manuel, P.; Callear, S. K.; Campbell, S. I.; Tang, C. C.; Schröder, M. Supramolecular binding and separation of hydrocarbons within a

https://doi.org/10.1021/jacs.1c10620
J. Am. Chem. Soc. 2022, 144, 1681−1689

functionalized porous metal−organic framework. *Nat. Chem.* **2015**, *7*, 121−129.
(72) Pei, J.; Wen, H. M.; Gu, X. W.; Qian, Q. L.; Yang, Y.; Cui, Y.; Li, B.; Chen, B.; Qian, G. Dense Packing of Acetylene in a Stable and Low-Cost Metal-Organic Framework for Efficient C_2H_2/CO_2 Separation. *Angew. Chem., Int. Ed.* **2021**, *60*, 25068−25074.
(73) Pei, J.; Shao, K.; Wang, J. X.; Wen, H. M.; Yang, Y.; Cui, Y.; Krishna, R.; Li, B.; Qian, G. A Chemically Stable Hofmann-Type Metal-Organic Framework with Sandwich-Like Binding Sites for Benchmark Acetylene Capture. *Adv. Mater.* **2020**, *32*, 1908275.
(74) Krishna, R. Metrics for Evaluation and Screening of Metal−Organic Frameworks for Applications in Mixture Separations. *ACS Omega* **2020**, *5*, 16987−17004.
(75) Krishna, R. Screening metal−organic frameworks for mixture separations in fixed-bed adsorbers using a combined selectivity/capacity metric. *RSC Adv.* **2017**, *7*, 35724−35737.
(76) Krishna, R. Methodologies for screening and selection of crystalline microporous materials in mixture separations. *Sep. Purif. Technol.* **2018**, *194*, 281−300.
(77) Zhang, Y.; Hu, J.; Krishna, R.; Wang, L.; Yang, L.; Cui, X.; Duttwyler, S.; Xing, H. Rational Design of Microporous MOFs with Anionic Boron Cluster Functionality and Cooperative Dihydrogen Binding Sites for Highly Selective Capture of Acetylene. *Angew. Chem., Int. Ed.* **2020**, *59*, 17664−17669.
(78) Wang, L.; Sun, W.; Zhang, Y.; Xu, N.; Krishna, R.; Hu, J.; Jiang, Y.; He, Y.; Xing, H. Interpenetration Symmetry Control Within Ultramicroporous Robust Boron Cluster Hybrid MOFs for Benchmark Purification of Acetylene from Carbon Dioxide. *Angew. Chem., Int. Ed.* **2021**, *60*, 22865−22870.
(79) Nijem, N.; Wu, H.; Canepa, P.; Marti, A.; Balkus, K. J., Jr.; Thonhauser, T.; Li, J.; Chabal, Y. J. Tuning the gate opening pressure of Metal-Organic Frameworks (MOFs) for the selective separation of hydrocarbons. *J. Am. Chem. Soc.* **2012**, *134*, 15201−15204.
(80) Mukherjee, S.; Kumar, N.; Bezrukov, A. A.; Tan, K.; Pham, T.; Forrest, K. A.; Oyekan, K. A.; Qazvini, O. T.; Madden, D. G.; Space, B.; Zaworotko, M. J. Amino-Functionalised Hybrid Ultramicroporous Materials that Enable Single-Step Ethylene Purification from a Ternary Mixture. *Angew. Chem., Int. Ed.* **2021**, *60*, 10902−10909.
(81) Maréchal, Y. *The Hydrogen Bond and the Water Molecule: The Physics and Chemistry of Water, Aqueous and Bio-Media*; Elsevier Science: 2007.
(82) Deacon, G. B.; Phillips, R. J. Relationships between the carbon-oxygen stretching frequencies of carboxylato complexes and the type of carboxylate coordination. *Coord. Chem. Rev.* **1980**, *33*, 227−250.
(83) Colthup, N. B.; Daly, L. H.; Wiberley, S. E. *Introduction to Infrared and Raman Spectroscopy*, 3rd ed.; Academic Press: 1990.
(84) Damasceno Borges, D.; Normand, P.; Permiakova, A.; Babarao, R.; Heymans, N.; Galvao, D. S.; Serre, C.; De Weireld, G.; Maurin, G. Gas Adsorption and Separation by the Al-Based Metal-Organic Framework MIL-160. *J. Phys. Chem. C* **2017**, *121*, 26822−26832.
(85) Henkelman, G.; Jónsson, H. Improved tangent estimate in the nudged elastic band method for finding minimum energy paths and saddle points. *J. Chem. Phys.* **2000**, *113*, 9978−9985.
(86) Henkelman, G.; Uberuaga, B. P.; Jónsson, H. A climbing image nudged elastic band method for finding saddle points and minimum energy paths. *J. Chem. Phys.* **2000**, *113*, 9901−9904.

https://doi.org/10.1021/jacs.1c10620
J. Am. Chem. Soc. 2022, 144, 1681−1689